Photoionization of the $3d$, $3p$, and $3s$ subshells of Zn I†

Arne W. Fliflet and Hugh P. Kelly
Department of Physics, University of Virginia, Charlottesville, Virginia 22901
(Received 13 August 1975)

The photoionization cross sections of the $3d$, $3p$, and $3s$ subshells of Zn I are calculated from threshold to 1000 eV. Electron-correlation effects are included using a low-order perturbation expansion obtained from many-body perturbation theory. The $3d \rightarrow kf$ cross section is also calculated in the exact single-channel random-phase approximation with exchange. Autoionizing resonances due to the $3p^5ns$ and $3p^5nd$ configurations are included in the $3d \rightarrow kf$ cross section, and the effect of core relaxation is considered. The effect of single-channel and multichannel correlations is included in all subshell cross sections.

I. INTRODUCTION

Results are presented for the photoionization cross section $\sigma(\omega)$ of the $3d$, $3p$, and $3s$ subshells of Zn I. Electron correlation effects are treated according to a prescription developed previously from many-body perturbation theory (MBPT).[1] The method involves the calculation of low-order diagrams in the random-phase approximation with exchange (RPAE).[2] Many-electron interactions among $4s$, $3d$, $3p$, and $3s$ electrons are included. Resonances in the $3d \rightarrow kf$ cross section due to the autoionizing configurations $3p^5ns$ and $3p^5nd$ are calculated.

There appear to be no accurate experimental data yet published for the photoionization of neutral zinc above 30 eV, so this work is a good example of an *a priori* calculation for a complex system. Several methods are used to test the accuracy of the results. The cross section is calculated in both length and velocity forms. Correlation energy effects are investigated by comparing results for the $3d \rightarrow kf$ cross section obtained using the (frozen-core) Hartree-Fock (HF) and the experimental $3d$ ionization energy. Core relaxation effects are estimated for the $3d \rightarrow kf$ cross section by means of a calculation using continuum orbitals calculated in the field of the Zn^+ $3d^9$ ion. The convergence of the perturbation expansion is checked by comparing it with the exact single-channel RPAE result for the case of the $3d \rightarrow kf$ cross section.

Section II outlines the prescription for $\sigma(\omega)$. The application of the RPAE effective interaction $\Gamma(\omega)$ to photoionization is also discussed. Resonances are calculated according to the MBPT prescription.[3] Section III describes the results emphasizing the $3d \rightarrow kf$ cross section which shows the largest effects.

II. THEORY

In previous work[1,3] a MBPT prescription was obtained for the calculation of $\sigma(\omega)$ for a closed-shell system with Hamiltonian

$$H = \sum_{i=1}^{N} \left(-\frac{1}{2} \nabla_i^2 - \frac{Z}{r_i} \right) + \sum_{i<j=1}^{N} v_{ij} , \tag{1}$$

where v_{ij} is the Coulomb interaction and atomic units are used. Amus'ya *et al.* have described the RPAE and have presented results for the rare gases.[2] To calculate $\sigma(\omega)$, the length L-form dipole matrix element

$$Z(p \rightarrow k) \equiv \langle \Psi(kp^{-1}) | \sum_i z_i | \Psi_0 \rangle , \tag{2}$$

is expanded in a series of open diagrams,[1] where Ψ_0 and $\Psi(kp^{-1})$ are exact many-particle ground and continuum states, and $\Psi(kp^{-1})$ results from the excitation of an electron from the ground-state orbital k. The velocity V form is obtained by replacing the matrix element in Eq. (2) by

$$-\langle \Psi(kp^{-1}) | \sum_i \frac{d}{dz_i} | \Psi_0 \rangle \Big/ (E_k - E_0) ,$$

where E_0 and E_k are energy eigenvalues for Ψ_0 and $\Psi(kp^{-1})$. Each diagram includes one dipole interaction and any number of interactions with the correlation perturbation

$$H_c' = \sum_{i<j=1}^{N} v_{ij} - \sum_{i=1}^{N} V(r_i) , \tag{3}$$

where $V(r_i)$ is the single-particle potential used to calculate the complete sets of orbitals that are used to evaluate the diagrams. The order of a diagram is taken to be the number of interactions with H_c'. Figure 1 shows examples of RPAE diagrams. The corresponding exchange diagrams are understood to be included.

The exact RPAE dipole matrix element is obtained by replacing the Coulomb interaction in diagrams 1(b) and 1(c) by the RPAE effective interaction $\Gamma(\omega)$ for ground-state correlations (GSC) and final-state correlations (FSC).[3] Matrix elements of $\Gamma(\omega)$ satisfy the equation[2]

$$\langle k_2k_4|\Gamma(\omega)|k_1k_3\rangle = -\left(\sum_{\substack{E_5\le E_F\\ E_6>E_F}} - \sum_{\substack{E_5>E_F\\ E_6\le E_F}}\right)\frac{\langle k_2k_6|\Gamma(\omega)|k_1k_5\rangle\langle k_5k_4|U|k_6k_3\rangle}{\omega - E_5 + E_6 + i\eta(1-2n_5)} + \langle k_2k_4|U|k_1k_3\rangle , \quad (4)$$

where k_i is a single-particle state with energy E_i, E_F is the Fermi energy, and

$$\langle k_2k_4|U|k_1k_3\rangle = \langle k_2k_4|v|k_1k_3\rangle - \langle k_2k_4|v|k_3k_1\rangle . \quad (5)$$

In the denominator of Eq. (4), the Fermi step function $n_5 = 1$ if k_5 is occupied in the ground state, $n_5 = 0$ if k_5 is an excited state. Figure 2 shows the coupled equations for the RPAE ground-state correlation (GSC) and final-state correlation (FSC) interaction amplitudes in diagrammatic notation. For photoionization, $\omega = E_{k_2} - E_{k_1}$. When $\Gamma(\omega)$ occurs above U in Fig. 2, the energy denominator is treated according to FSC.[3] The energy denominator does not involve the states k_3 and k_4.

The RPAE equations for the case of single-channel correlations simplify considerably when the Hartree-Fock HF V^{n-1} (^1P) potential is used. As pointed out by Amus'ya *et al.*,[2] this potential cancels the lowest-order single-channel FSC interaction. Strictly speaking, this cancellation violates the exclusion principle when more than two hole-particle pairs are excited.[4] However, this effect involves a small correction to diagrams which are themselves small, and hence it may be neglected. Using the HF V^{n-1} (^1P) potential eliminates the second term on the right-hand side (RHS) of Fig. 2(a) and the first and third terms on the RHS of Fig. 2(b). The nonvanishing single-channel RPAE diagrams through second order are diagrams 1(a), 1(b), 1(d), and 1(e). Diagram 1(c) is canceled by the HF V^{n-1} (^1P) potential.[2,3] The single-channel RPAE interaction amplitudes are obtained by using techniques developed for evaluating diagrams[5-7] to express Eq. (4) in matrix form. The equation is then solved by matrix inversion.

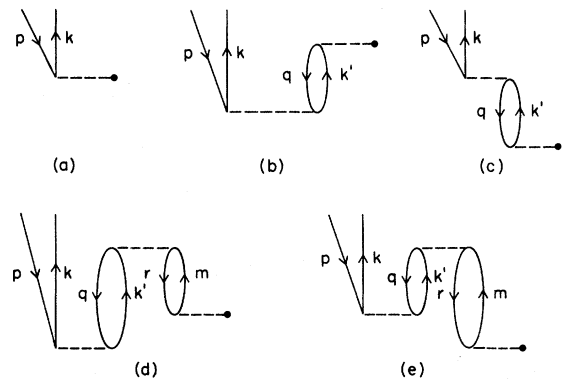

FIG. 1. RPAE diagrams occurring in the perturbation expansion for $\langle \Psi(kp^{-1})|\sum_i Z_i|\Psi_0\rangle$. Solid dots indicate dipole interactions, other dashed lines indicate Coulomb interactions. Time increases upwards. Exchange diagrams are not shown.

The RPAE omits many diagrams that are second order in H_c'. These diagrams account for modification of the atomic wave function owing to relaxation and polarization of the core during ionization, and configuration interaction effects. Other diagrams neglected by the RPAE contribute to the correlation energy of the atom. The length and velocity forms of the dipole matrix element agree in the RPAE, but they do not agree when correlation energy corrections are included without including the corresponding diagrams which modify the wave function. In this work, correlation energy effects are approximately included by using experimental removal energies for the ground-state orbitals.[1,3] This gives the photoionization threshold correctly, and the discrepancy between the length and velocity forms of the cross section is a measure of the effect of extra RPAE diagrams. Normalization diagrams[6] are also omitted by the RPAE. However, they may be essentially included by means of an over-all factor in the cross section.[3]

Frozen-core[3] single-particle potentials are used except as noted. The Silverstone-Huzinaga projection operator[8,9] is added when necessary to ensure orthogonality of excited orbitals to ground-state orbitals.

III. RESULTS

For Zn I the $3d \rightarrow kf$ cross section has the largest single-channel correlation effects and is the case used to check the convergence of the diagrammatic expansion. The expansion consists of single-channel RPAE diagrams through second order. To iso-

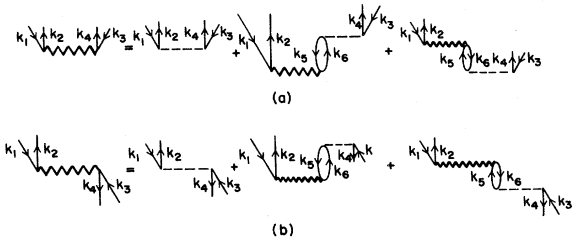

FIG. 2. Coupled equations for RPAE GSC and FSC amplitudes of $\Gamma(\omega)$, which are indicated by sawtooth lines. The dashed lines indicate amplitudes of U.

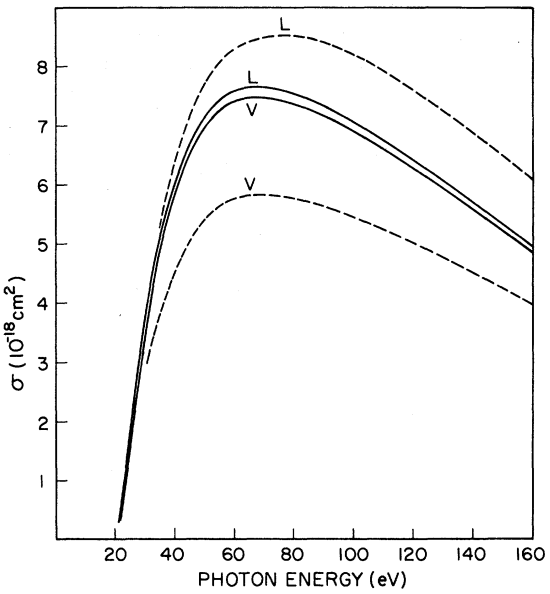

FIG. 3. Photoionization cross section $\sigma(\omega)$ for $3d \rightarrow kf$ calculated using the frozen-core HF $3d$ removal energy. The dashed curves labeled L and V represent the HF length-land velocity-form results. The solid curves indicate single-channel correlation results both in the exact RPAE and for our diagrammatic expansions of the RPAE.

late the effect of RPAE correlations the (frozen-core) HF $3d$ removal energy (21.29 eV) is used in the diagrams and in the RPAE equation. Figure 3 shows the HF and RPAE results for the $3d \rightarrow kf$ cross section. The diagrammatic expansion and exact RPAE results differ by less than 1%, and both are represented by the solid curves labeled L and V for the length and velocity forms. The HF results are shown by the dashed curves. The discrepancy between the RPAE L and V curves is attributed to errors in the numerical approximation. As pointed out in a previous work,[10] the effect of single-channel GSC is to bring the L and V velocity forms together. Single-channel FSC usually increase both forms in the region of the cross-section maximum and decrease them at higher photon energy. In the present case most of the correlation effect is due to GSC; the effect of FSC is small.

Figure 4 shows results for the $3d \rightarrow kf$ cross section obtained using the experimental $3d$ removal energy[11] (17.30 eV). Again, the exact and diagrammatic expansion RPAE results differ by less than 1% and are both represented by the solid curves labeled L and V, which indicate the length- and velocity-form cross sections. The corresponding HF results are shown by the dotted curves. As expected from the discussion in the preceding section, the RPAE L and V results do not agree, and are inverted with respect to the HF results. This behavior is due to σ_L being roughly proportional to the removal energy near threshold, whereas σ_V is inversely proportional.

To study how the discrepancy between the RPAE L and V cross sections is related to core relaxation effects, results have been obtained for diagrams computed using continuum orbitals calculated in the field of the self-consistent Zn^+ $3d^9$ ion. The dashed curves, labeled L and V in Fig. 4, show these results. The agreement between σ_L and σ_V is improved in the region of the cross-section maximum; however, there is little change near threshold, and at higher photon energy the agreement becomes worse. The latter discrepancy may reflect the fact that at high energy the photoelectron is ejected before the core relaxes. On the other hand, for photon energies near threshold, continuum orbitals do not penetrate the core orbitals because of the centrifugal barrier and hence are relatively insensitive to relaxation effects in the core orbitals.

Interchannel correlation effects are included by calculating diagrams 1(b) and 1(c). Interaction of the $3d \rightarrow kf$ channel with the following channels is included: $3d \rightarrow kp$, $4s \rightarrow kp$, $3p \rightarrow kd$, $3p \rightarrow ks$, and $3s \rightarrow kp$. The diagrams are calculated using the experimental electron-removal energies[11,12]: E_{4s}

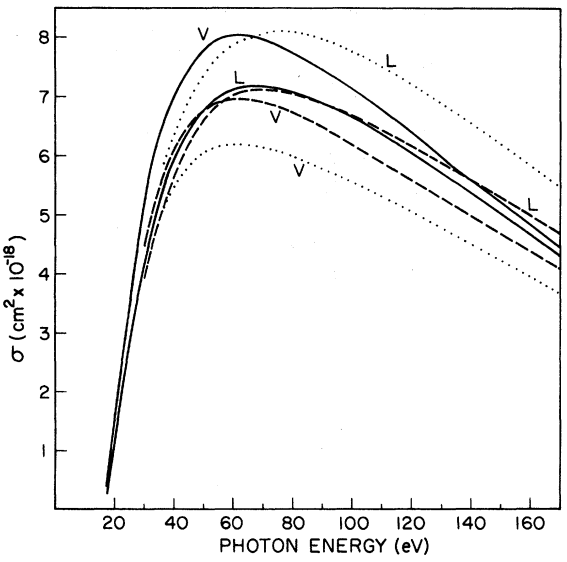

FIG. 4. Results for the $3d \rightarrow kf$ cross section $\sigma(\omega)$ calculated using the experimental HF $3d$ removal energy. The dotted curves represent the length and velocity HF results; the solid curves indicate the exact RPAE and diagrammatic expansion results, and the dashed curves indicate diagrammatic RPAE results obtained using orbitals calculated in a relaxed core potenial.

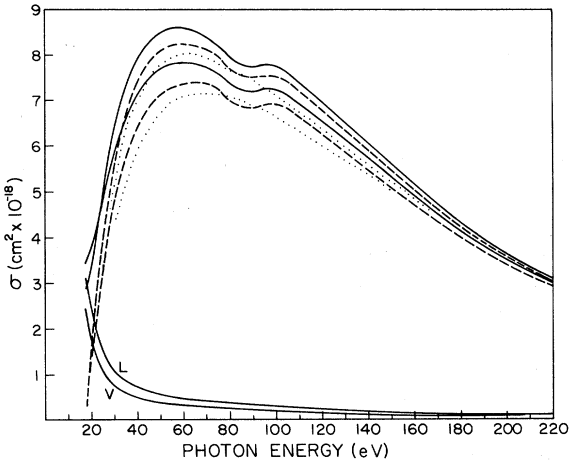

FIG. 5. The solid curves labeled L and V are correlated results for the $3d \rightarrow kp$ cross section. The dashed curves are the $3d \rightarrow kf$ cross section including single-channel and inter-channel RPAE correlations; the upper curve in each case is the velocity form. The dotted curves show the $3d \rightarrow kf$ cross section including single-channel correlations for comparison. The unlabeled solid curves represent the total $3d$ cross section including correlations.

$= 9.39$, $E_{3p} = 87.1$, and $E_{3s} = 137.0$ eV. Results for the RPAE $3d \rightarrow kf$ cross section including single-channel and interchannel correlations are shown in Fig. 5. The fully correlated L and V cross sections are indicated by the dashed curves. The V form lies above the L form. The dotted curves show the single-channel results for comparison (the upper curve shows the V form). The fully correlated results have an interesting structure in the region near the onset of the $3p$ cross section. The series of narrow resonances in this region that are due to the autoionizing configurations $3p^5ns$ and $3p^5nd$ are not shown. These resonances have little effect on the average behavior of the cross section and are discussed below. The structure between 70 and 110 eV is caused by diagram 1(c) with $p, k = 3d, kf$ and $q, k' = 3p, k'd$ and $k's$, where k' denotes continuum orbitals only. The effect is not sensitive to the contribution from high-n bound states, which are included by extrapolation of the continuum. Similar structure, although much smaller in magnitude, occurs near the onset of the $3s$ cross section owing to diagram 1(c) with $q, k' = 3s, k'p$.

TABLE I. Autoionizing resonance parameters.

State	E_n (eV)	q_n (a.u.)	$\Gamma_n/2\times10^5$ (a.u.)	$f_n\times10^2$
$3p^6 5s$	83.7	16.4	3.58	7.72
$6s$	85.7	16.4	0.532	1.15
$7s$	86.3	16.5	0.210	0.455
$3p^5 4d$	85.5	0.949	15.3	0.0550
$5d$	86.2	0.904	7.57	0.0247
$6d$	86.5	0.873	4.11	0.0125

Resonances in the $3d \rightarrow kf$ cross section arising from the $3p^5ns$ and $3p^5nd$ configurations are calculated using a MBPT prescription[3] which is essentially equivalent to Fano's configuration-interaction theory for many discrete states and one continuum channel.[13] Diagram 1(c) with $p, k = 3d, kf$ and $q, k' = 3p, ns$ and nd represents the lowest-order contribution to the resonance diagrams. The $3p \rightarrow ns$ and $3p \rightarrow nd$ dipole matrix elements and the resonance half-widths are calculated in the frozen-core HF approximation, and the spin-orbit interaction is neglected. Figure 6 shows the L-form

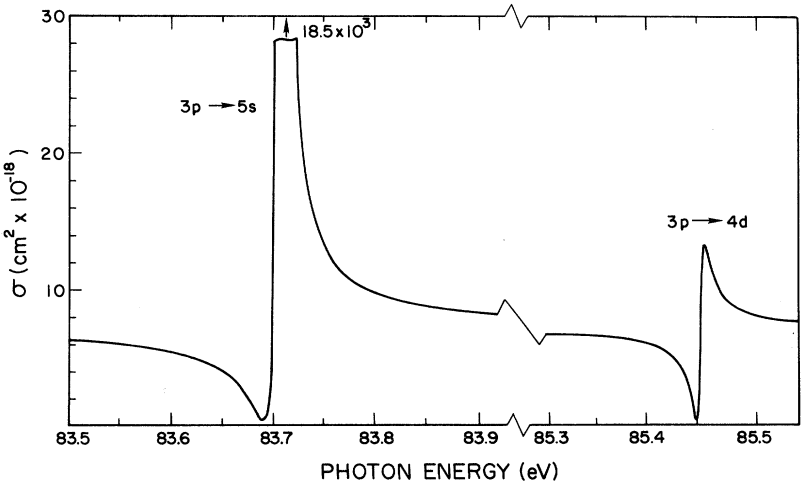

FIG. 6. Photoionization cross section $\sigma(\omega)$ for the $3d$ subshell in the region of $3p^5 5s$ and $3p^5 4d$ autoionizing resonances. The curves show the length-form results.

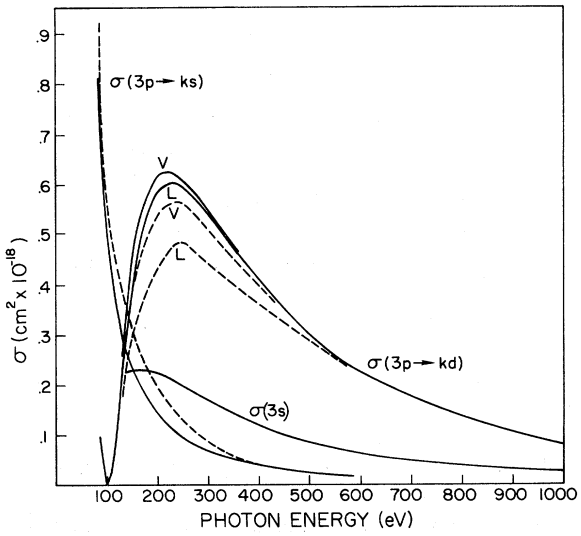

FIG. 7. Photoionization cross sections for $3p$ and $3s$ subshells. The solid curves for the $3p \rightarrow kd$ cross section are HF L- and V-form results; the dashed curves are the results including correlations. The dashed $3p \rightarrow ks$ curve is the correlated L-form result; the solid curve is the HF L-form result. The σ_{3s} curves indicate the correlated L-form result.

cross section in the region of the $3p^5 5s$ and $3p^5 4d$ resonances. The curves include the contribution from the $3d \rightarrow kp$ cross section discussed below; however, autoionization in the $3d \rightarrow kp$ channel is not considered. Table I shows calculated values for several resonances of the resonance energy E_n, the Fano profile parameter[13] q_n, the half-width $\frac{1}{2}\Gamma_n$, and the oscillator strength f_n of the autoionizing configuration.

Calculations including first-order RPAE correlations with the channels listed above have been carried out for the other $n = 3$ subshell cross sections. Figure 5 shows correlated results for the $3d \rightarrow kp$ cross section which are represented by the solid curves labeled L and V. Figure 5 also shows L and V curves for the total correlated $3d$ subshell cross section (excluding resonance effects). These curves are indicated by the unlabeled solid curves, with the upper curve representing the V form (except near threshold). The HF results for the $3d \rightarrow kp$ cross section lie about 20% below the curves shown in Fig. 5 at threshold, but are in good agreement at higher energies. Curves for the $3p \rightarrow kd$, $3p \rightarrow ks$, and $3s \rightarrow kp$ cross sections are shown in Fig. 7. The solid curves for the $3p \rightarrow kd$ cross section indicate the HF L and V results; the dashed curves indicate the RPAE results. Comparison of these curves shows that the principal correlation effect in the $3p \rightarrow kd$ cross section is an approximately 15% decrease in the maximum. In this case the agreement between the L and V curves becomes worse when correlations are included. This discrepancy is attributed to the omission of diagrams corresponding to core relaxation. The solid curve in Fig. 7 for the $3p \rightarrow ks$ cross section represents the HF L-form results; the corresponding dashed curve shows the RPAE L result. The V-form cross sections are about 10% larger at threshold but are otherwise well represented by the $3p \rightarrow ks$ curves shown. Only the HF L result is shown for the $3s \rightarrow kp$ cross section. This curve is in good agreement with both the HF V-form result and the RPAE results.

The $4s$-kp cross section is negligible at the onset of the $3d$ cross section. Normalization diagrams are estimated to decrease the total cross section by about 1% above the $3d$ threshold, and are neglected. The solid curves in Fig. 8 show the total L and V cross sections for Zn I from

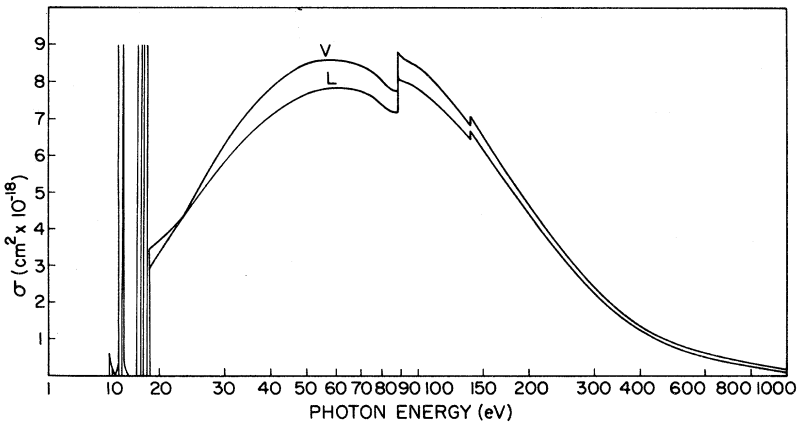

FIG. 8. Total photoionization cross section of Zn from threshold to 1 keV. Curve below 17.3 eV is V-form of the $4s$ subshell cross section from Ref. 3. The $3d^9 np$ resonances are indicated approximately and are severely truncated. Other resonances are not shown.

threshold up to 1000 eV. Below 17.30 eV, the curve shows the $4s$ subshell V-form cross section obtained previously.[3] The $3d^9np$ resonances are shown approximately and are severely truncated. The results for the $n=3$ subshell cross sections are in qualitative agreement with an RPAE calculation by Amus'ya *et al.*,[14] and are also consistent with experimental data obtained by Harrison *et al.*[15] and by Connerade.[16] The experimental data of Harrison *et al.* peaks at 38 eV, about 20 eV below our result. However, our results are within the experimental error bars, which are large for the upper range of data.[15]

IV. DISCUSSION AND CONCLUSIONS

Results for the $3d \rightarrow kf$ cross section show that the convergence of the diagrammatic expansion for the RPAE is very good in that case. The discrepancy between RPAE L and V cross sections when the experimental removal energy is used (which approximately accounts for correlation-energy shifts) indicates the importance of correlation effects outside the RPAE. It seems reasonable to expect that these effects are adequately represented by second-order diagrams.

From the calculation of $\sigma(3d \rightarrow kf)$ using excited orbitals calculated in an ionic core potential, it is probable that core relaxation effects account for a substantial amount of the discrepancy between the RPAE L and V curves in the region of the cross-section maximum. An explicit diagrammatic calculation is needed to verify this effect.

The rapid variation in the slope of the $3d \rightarrow kf$ cross section that is due to correlation with $3p$ electrons appears to be a physical effect rather than an artifact of the diagrammatic prescription. Tests indicate that this structure is not due to the $3p^5ns$ and $3p^5nd$ resonances which occur in this region (not shown in Fig. 6). Also, one expects structure arising from these resonances to affect a much narrower region.

The calculations for the $3p$ and $3s$ subshell cross sections indicate that correlation effects become smaller for more tightly bound electrons. This reflects the increasing dominance of the nuclear attraction term in the potential for inner electrons.

Table I shows that the $3p^5ns$ resonances have much more oscillator strength than the $3p^5nd$ resonances. This is consistent with the rule that the oscillator strength of $l \rightarrow l+1$ transition is primarily in the continuum whereas $l \rightarrow l-1$ transitions have less continuum oscillator strength.

These calculations indicate that the cross-section maximum for Zn I occurs about 20 eV above the 38-eV measurement by Harrison *et al.*[15] Near the $3d$ electron threshold we expect structure owing to two-electron resonances involving $4s$ and $3d$ electrons. These effects will be considered in future work. In addition, we intend to investigate the contribution from two-electron photoionization in this region.

---

†Work supported by the National Science Foundation.

[1]H. P. Kelly and A. Ron, Phys. Rev. A 5, 168 (1972).
[2]M. Ya. Amus'ya, N. A. Cherepkov, and L. V. Chernysheva, Zh. Eksp. Teor. Fiz. 60, 160 (1971) [Sov. Phys.–JETP 33, 90 (1971)].
[3]A. W. Fliflet and H. P. Kelly, Phys. Rev. A 10, 508 (1974).
[4]G. Wendin, J. Phys. B 5, 110 (1972).
[5]H. P. Kelly, Phys. Rev. 131, 684 (1963).
[6]H. P. Kelly, Phys. Rev. 136, 3896 (1964).
[7]H. P. Kelly, Phys. Rev. 144, 39 (1966).
[8]H. J. Silverstone and M. L. Yin, J. Chem. Phys. 49, 2026 (1968).
[9]S. Huzinaga and C. Arnau, Phys. Rev. A 1, 1285 (1970).
[10]A. W. Fliflet, R. L. Chase, and H. P. Kelly, J. Phys. B 7, L443 (1974).
[11]C. E. Moore, *Atomic Energy Levels*, Natl. Bur. Std. Circ. No. 467 (U. S. GPO, Washington, D. C., 1949).
[12]K. Siegbahn *et al.*, *Atomic, Molecular, and Solid State Structure Studied by Means of Electron Spectroscopy* (Almqvist and Wilksells, Uppsala, Sweden, 1967).
[13]U. Fano and J. W. Cooper, Phys. Rev. 137, A1364 (1965).
[14]M. Ya. Amus'ya, N. A. Cherepkov, and L. V. Chernysheva, in *Proceedings of the Eighth International Conference on the Physics of Electronic and Atomic Collisions, Belgrade, Yugoslavia, July 1973*, edited by B. C. Čobić and M. V. Kurepa (Institute of Physics, Belgrade, Yugoslavia, 1973), p. 196.
[15]H. Harrison, R. I. Shoen, and R. B. Cairns, J. Chem. Phys. 50, 3930 (1969).
[16]J. P. Connerade (private communication).